^{4}He adsorbed outside a single carbon nanotube

M. C. Gordillo

Departamento de Sistemas Físicos, Químicos y Naturales, Facultad de Ciencias Experimentales, Universidad Pablo de Olavide, Carretera de Utrera, km 1, 41013 Sevilla, Spain

J. Boronat

Departament de Física i Enginyeria Nuclear, Universitat Politècnica de Catalunya, B4-B5 Campus Nord, 08034 Barcelona, Spain

(Received 6 June 2012; revised manuscript received 6 September 2012; published 8 October 2012)

The phase diagrams of ^{4}He adsorbed on the external surfaces of single armchair carbon nanotubes with radii in the range 3.42–10.85 Å are calculated using the diffusion Monte Carlo method. For nanotubes narrower than a (10,10) one, the ground state is an incommensurate solid similar to the one found for H_2 on the same substrates. For wider nanotubes, the phase with the minimum energy per particle is a liquid layer. Curved $\sqrt{3} \times \sqrt{3}$ registered solids similar to the ones found on graphene and graphite were unstable for all the tubes considered.

DOI: 10.1103/PhysRevB.86.165409 PACS number(s): 68.90.+g, 05.30.−d

I. INTRODUCTION

Until recently, the only experimental studies about the adsorption of quantum gases (^{4}He, H_2, and Ne) on carbon nanotubes were performed in tube associations called bundles.[1–7] In these structures, the only places available for adsorption are their outer surfaces, in particular the grooves between two adjacent tubes.[8] Other possible locations are the triangular interstices among three neighboring tubes in the bulk part of the bundle. However, those places seem to be not populated.[2,3,9] The other option is the adsorption on the inner surface of nanotubes, but to do so one has to remove the caps that close them at the ends. To our knowledge, there is no experimental data on this possibility for quantum gases, the only studies being up to now theoretical.[11–15]

A recent experimental work showed that it is possible to isolate a single carbon nanotube and adsorb Ar and Kr on its outer surface.[10] The experimental phase diagrams for these classical noble gases were qualitatively similar to those on graphite. For instance, they include a $\sqrt{3} \times \sqrt{3}$ phase for Ar on tubes whose diameters are in the range 1–3 nm. However, recent quantum Monte Carlo simulations[16] of H_2 adsorbed on nanotubes with diameters between ∼7 and 22 Å indicate that this structure was formed only on the widest tube considered, a (16,16) one in the standard nomenclature.[17] In opposition to what happens on flat surfaces, mainly graphite, in which the phase diagrams of quantum gases are quite well known from both theory and experiment, adsorption on curved surfaces is much less studied. Apart from studies related to wetting transitions of classical gases on cylinders and spheres,[18,19] the possible new phases that curvature can produce in quantum gases are still rather unknown[20] and it is plausible to imagine that experiments on isolated nanotubes exposed to quantum gases in the near future.

In this work, we have used the diffusion Monte Carlo (DMC) method to obtain the phase diagrams of ^{4}He adsorbed on isolated carbon nanotubes with radii ranging between 3.42 and 10.85 Å. These correspond to armchair nanotubes between (5,5) and (16,16) in the standard nomenclature. Our main aim is to compare our results with both the ones for H_2 on the same surface[16] and those for ^{4}He on graphene,[21] a flat surface that can be considered a tube of infinite radius.

The rest of the paper is structured as follows. In the next section, we describe the DMC algorithm used to solve the corresponding Schrödinger equations from which we inferred the corresponding phase diagrams. The phase diagrams themselves will be shown in Sec. III, and the paper will close by summarizing our main conclusions in Sec. IV.

II. METHOD

The diffusion Monte Carlo method allows for solving the many-body Schrödinger equation exactly if the constituents of the system are bosons,[22] as it is the case of ^{4}He atoms. Since it is a stochastic method, the results are always produced with some statistical uncertainties. The different carbon nanotubes were considered as rigid cylinders in which the individual carbon positions were kept constant throughout the simulation. The interaction between any of those carbons and each helium atom was of the Lennard-Jones type with parameters taken from Ref. 23, i.e., the carbon-helium interactions act as an external potential to be included in the Schrödinger equation to solve. The helium-helium interparticle interaction was taken to be a standard Aziz potential.[24]

DMC solves the N-body Schrödinger equation in imaginary time. The walkers (sets of $3N$ coordinates) representing the system evolve in time through a diffusion process and an energy selection rule named branching. In order to reduce the statistical variance, the free diffusion movement is corrected by a drift term that enhances the sampling in regions where the exact wave function is expected to be reasonably large. Technically, this importance sampling is implemented by introducing a guiding wave function which avoids the sampling inside the cores of the interaction and fixes the phase of the system under study. In particular, for an adsorbed liquid layer, we use

$$\Phi(\mathbf{r}_1,\mathbf{r}_2,\ldots,\mathbf{r}_N) = \prod_{i<j} \exp\left[-\frac{1}{2}\left(\frac{b_{\mathrm{He-He}}}{r_{ij}}\right)^5\right] \prod_i \Psi(r_i), \tag{1}$$

where $\mathbf{r}_1,\mathbf{r}_2,\ldots,\mathbf{r}_N$ are the ^{4}He positions. The first part of the product in Eq. (1) is the Jastrow function that depends on the distances r_{ij} between the atoms. There, $b_{\mathrm{He-He}}$, is a

TABLE I. The set of armchair carbon nanotubes considered in this work and their tube radii (r_t) together with the helium adsorption energy (e_0) in the infinite dilution limit. Also included for comparison is the same value for graphene, taken from Ref. 21. r_0 is the most probable distance of a single ^{4}He atom to the center of the tube.

Tube	r_t (Å)	r_0 (Å)	e_0 (K)
(5,5)	3.42	6.26	-94.76 ± 0.06
(6,6)	4.10	6.93	-97.4 ± 0.2
(8,8)	5.45	8.26	-100.94 ± 0.09
(10,10)	6.80	9.65	-103.29 ± 0.08
(12,12)	8.14	11.01	-104.72 ± 0.04
(14,14)	9.49	12.37	-105.22 ± 0.07
(16,16)	10.85	13.70	-104.98 ± 0.06
graphene (Ref. 21)	∞	...	-141.64 ± 0.01

variational parameter fixed at 3.07 Å.[21] $\Psi(r_i)$ is the same one-body function than the one used in Ref. 21, whose role is to radially confine the moving particles around the minimum of the collective sum of all C-He interactions. To do so, it has a maximum at a distance of ∼2.87 Å from the surface of the different tubes and decreases monotonously both for larger and smaller separations.

When the cylinder is coated with a solid layer, we introduce in the trial wave function a factor,

$$\prod_i \exp\{-c[(x_i - x_{\rm site})^2 + (y_i - y_{\rm site})^2 + (z_i - z_{\rm site})^2]\}\ , \tag{2}$$

that multiplies the Jastrow part [see Eq. (1)]. With this approach, each helium atom is mainly sampled in the vicinity of its associated crystallographic position $x_{\rm site}, y_{\rm site}, z_{\rm site}$. The value of the c parameter for the different solid phases were the same as the ones used for the same phases in a previous simulation on graphene.[21]

III. RESULTS

The nanotubes considered in this work, together with their respective radii (distance from the center of the tube to the carbon surface) and the energy per particle in the infinite dilution limit, e_0, are shown in Table I. Those energy values were obtained from simulations including a single helium atom on a tube 70-Å long. What we observe is that, in general, e_0 increases with the tube radius, but it is far from the value of a flat surface. In Table I, r_0 is the most probable radial distance of a single helium atom to the center of each tube. In the remaining of the paper, all the adsorbate densities will be calculated using that distance as the radius of the helium cylinder that coats the carbon nanotube.

There is no simple explanation for the evolution of e_0 as a function of the tube radius beyond the general increase when it grows. For instance, e_0 is slightly lower for the (14,14) tube than for the (16,16) one. To try to understand this effect and its connection with the curvature of the adsorbing surface, we calculated the difference in the potential energy felt by a helium particle located 2.87 Å above the center of one of the hexagons that conform the tube (c) and for an atom located above the center of a C-C bond (s) at the same height. This difference is an estimation of the corrugation of the potential surface. In graphene, a flat structure, those values are $V_c = -175.02$ and $V_s = -167.49$ K. This means a difference of 7.53 K. That is a measure of the energy barrier that ^{4}He atoms have to jump in order to explore the graphene surface. The corresponding average potential energy from a full DMC calculation of a single helium on that structure is -151.43 ± 0.05 K, what indicates that the particle explores also less favorable positions. The respective pairs of potential energies for the tubes under consideration are $V_c = -154.35$ and $V_s = -147.57$ K (a difference of 6.79 K) for the (14,14) tube, to be compared to $V_c = -156.32$ and $V_s = -148.19$ K (8.13 K) for the (16,16) one. The DMC potential energy averages are -125.7 ± 0.1 and -125.6 ± 0.1 K, respectively, i.e., virtually identical. This means that simply summing up the He-carbon interactions in a reduced number of positions is not a precise guide neither for e_0 nor for the average potential interaction. The corrugation effect in a single carbon hexagon is similar for a planar and for a curved environment but the potential energy and e_0 are smaller (in absolute value) than in planar graphene because the curved adsorbent is globally less attractive.

To study the possible helium phases on each carbon cylinder, we follow closely a previous study of H_2 adsorbed on the same systems (see Ref. 16). Liquid phases, i.e., helium arrangements described by Eq. (1), and curved counterparts of the registered $\sqrt{3} \times \sqrt{3}$ phases have been considered.[10] Structures with helium atoms regularly distributed on circumferences (or rows) whose defining planes were perpendicular to the main axis (z) of the cylinders were also studied. Those solids are defined by the number of absorbed atoms on each circle and are named accordingly. For instance, if we have ten atoms on the outside of the circle, the phase is termed a ten-in-a-row solid. The densities were determined by the distances between neighboring circumferences along the z axis. Those rows were rotated half the distance between helium atoms with respect to each other to maximize the number of closest neighbors for each helium atom. For completeness, the wrapped up equivalents to the 3/7 and 2/5 registered structures proposed by Greywall[25] for graphite were also taken into account.

Figure 1 shows the phase diagram of ^{4}He adsorbed on the surface of a (5,5) tube. We observe that, as in the case of H_2 adsorbed on the same cylinder,[16] the ground state is not a liquid (open squares), but a structure corresponding to a five-in-a-row solid (full squares). The minimum energy per particle is -96.10 ± 0.03 K with a density $\rho = 0.0620 \pm 0.0002$ Å^{-2}, as can be seen in Table II. These results, as the ones corresponding to incommensurate solids on other tubes, were extracted from a third-order polynomial fit to the simulation results around the point of the minimum energy; in this particular case, to the six points corresponding to the lowest densities of the set of full squares in Fig. 1. The error bars in Table II were also obtained from the least-squares fit. $\rho = 0.0620$ Å^{-2} is the lowest density for which a solid is stable; below it, the system will form a patch of that solid and leave the rest of surface of the tube empty. On the other hand, when the amount of adsorbed helium increases, the energy per particle of this five-in-a-row structure is above the corresponding to a six-in-a-row incommensurate solid (full circles in Fig. 1). This means

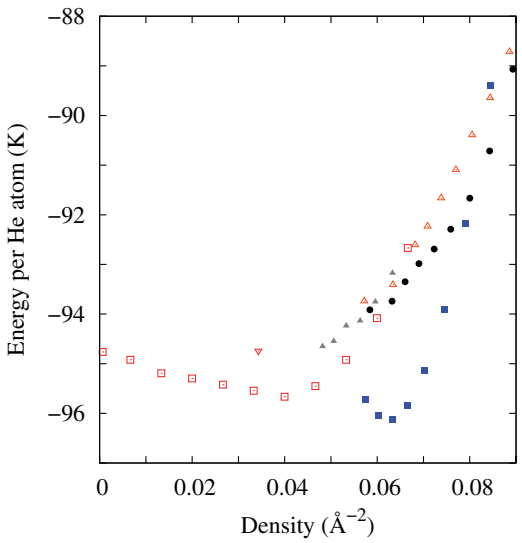

FIG. 1. (Color online) Energy per helium atom for different phases adsorbed on a (5,5) tube. Open squares, liquid phase; full squares, a five-in-a-row atom solid incommensurate phase; full circles, six-in-a-row arrangement; open up triangles, incommensurate solid with seven atoms per row; up full triangles, solid of the same type with four atoms per circumference. The open down triangle indicates the result for a curved $\sqrt{3} \times \sqrt{3}$ structure.

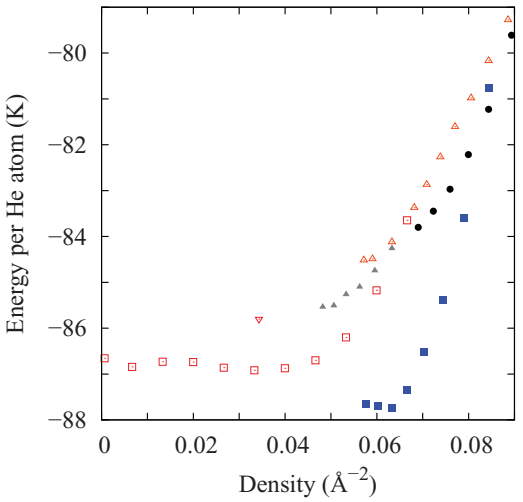

FIG. 2. (Color online) Same that in the previous figure, but using as a C-He potential the anisotropic expression of Carlos and Cole (see Ref. 27).

that the system should undergo a first-order phase transition between those arrangements. By means of a double-tangent Maxwell construction considering both the full squares and full circles in Fig. 1, we found that the transition region is between 0.0752 ± 0.0002 Å^{-2} (upper density limit for a five-in-a-row structure) and 0.0845 ± 0.0002 Å^{-2} (lower density for which a six-in-a-row structure is stable). Their respective energies per particle are -93.67 ± 0.01 and -90.63 ± 0.01 K. To estimate these energies and densities, we used the simulation results and interpolated between them a set of third-order polynomial splines. This means that no particular polynomial fit for any of the equations of state (represented here by the complete set of simulation points) was used. None of the other arrangements considered (liquid, registered $\sqrt{3} \times \sqrt{3}$ solid, or other commensurate structures) are stable, since their energies per particle are larger than the corresponding to any of the above mentioned structures (see Fig. 1 and Table II). For the registered solids whose data are given in Table II, the densities are given as exact values, since a pure commensurate structure forms only at a characteristic density. The error bars of the energies per particle are the statistical uncertainties derived from their respective diffusion Monte Carlo calculations.

The phase diagram for a (6,6) tube is similar to the already described for the (5,5) one: the ground state is a six-in-a-row structure whose minimum density obtained from the same type of third-order polynomial fit to the simulation results around the minimum of energy, is 0.0658 ± 0.0005 Å^{-2}. Upon a density increase, this solid structure suffers a first-order phase transition at $\rho = 0.0836 \pm 0.0002$ Å^{-2} (energy per particle, -95.68 ± 0.03 K) to a seven-in-a-row solid with $\rho = 0.0843 \pm 0.0003$ Å^{-2} (energy per particle, -91.78 ± 0.02 K). That none of the other commensurate or liquid phases are stable can be checked in Table II: all of them have energies per particle greater that the one for the ground state.

To obtain the data displayed in Fig. 1, we have used the isotropic C-He interaction of Stan and Cole (see Ref. 23). This was the interaction used in previous studies of helium adsorbed on carbon nanotubes (see, for instance, Refs. 11,12,15, and 26). However, there is another possibility: an anisotropic form of the same interaction proposed by Carlos and Cole.[27] The DMC results with this latter interaction are displayed in Fig. 2 and

TABLE II. Energies per particle (e_b) and equilibrium helium densities (ρ) for nanotubes in which the ground state is an incommensurate solid. The error bars are given in parenthesis and affect to the last figure shown. The commensurate solid arrangements are represented by a single density without error bars. The results labeled with a * were obtained using the anisotropic potential of Ref. 27 instead of the isotropic interaction employed in the other cases.

Phase	liquid		2/5		3/7		$\sqrt{3} \times \sqrt{3}$		incommensurate solid	
Tube	ρ (Å^{-2})	e_b (K)	ρ (Å^{-2})	e_b (K)	ρ (Å^{-2})	e_b (K)	ρ (Å^{-2})	e_b (K)	ρ (Å^{-2})	e_b (K)
(5,5)	0.0364(7)	− 95.66(3)	0.0410	− 95.07(8)	0.0439	− 94.63(8)	0.0341	− 94.74(3)	0.0620(2)	− 96.10(3)
(5,5)*	0.0364(5)	− 86.94(2)	0.0410	− 86.70(8)	0.0439	− 85.93(7)	0.0341	− 85.81(3)	0.0598(2)	− 87.76(5)
(6,6)	0.0356(2)	− 98.65(6)	0.0444	− 97.81(6)	0.0475	− 97.07(7)	0.0369	− 97.01(4)	0.0658(5)	− 99.05(4)
(8,8)	0.0358(1)	− 102.02(2)	0.0495	− 101.49(4)	0.0529	− 100.56(4)	0.0412	− 101.00(4)	0.0744(9)	− 102.50(2)
(10,10)	0.0323(9)	− 104.20(2)	0.0534	− 103.74(5)	0.0573	− 102.78(3)	0.0445	− 103.36(3)	0.0730(7)	− 104.15(4)
(10,10)*	0.0373(1)	− 98.31(2)	0.0534	− 98.12(5)	0.0573	− 96.65(5)	0.0445	− 97.93(5)	0.0783(4)	− 98.88(4)

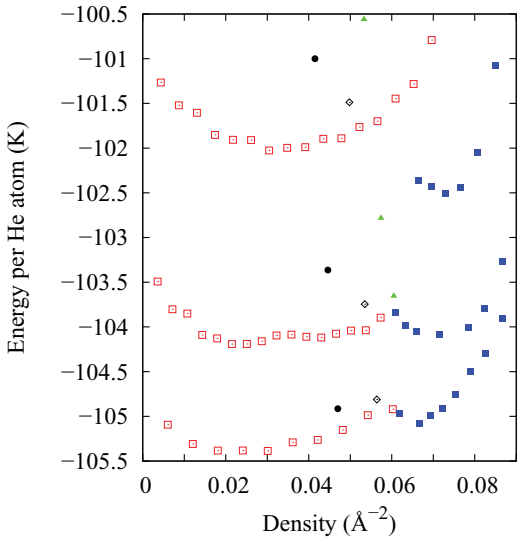

FIG. 3. (Color online) Energy per particle as a function of density for liquid (open squares), incommensurate (full squares), $\sqrt{3} \times \sqrt{3}$ (full circle), 3/7 (full triangles), and 2/5 (open diamonds) phases. The upper set of symbols corresponds to a (8,8) tube, the middle set to a (10,10) tube and the lowest to a (12,12) cylinder.

Table II. From them, one can see that the ground state is still a five-in-a-row solid whose minimum stable density is ∼3.5% lower than the one for the isotropic potential. The energies per particle in the anisotropic case are ∼8.7 K larger due to a slight decrease of its potential well depth with respect to the isotropic model. However, there is no way to discriminate between the two sets of parameters since, to our knowledge, there is not available experimental information to compare our simulations to. Our results show that with the anisotropic interaction there is also a first-order phase transition at $\rho = 0.0787 \pm 0.0001$ Å^{-2} (energy per particle, -83.77 ± 0.01 K) to a six-in-row solid whose lowest density is 0.0883 ± 0.0001 Å^{-2} and the energy per particle is -80.07 ± 0.02 K. This means that the transition region is shifted to larger densities. We can also see in Table II that the anisotropic interaction favors the incommensurate solid with respect to the liquid: the energy per particle difference between the ground state and the liquid minimum is 0.44 ± 0.04 K for the isotropic potential and 0.82 ± 0.05 K for the anisotropic one.

The phase diagram of the (8,8) tube is qualitatively similar to those of the thinner tubes already described. Its ground state is an incommensurate solid of the type n-in-a-row, were n is the nanotube index ($n = 8$). The main difference is that in the density range considered (up to ∼0.10 Å^{-2}), there is only one stable incommensurate structure, i.e., there is no first-order transition between two incommensurate solids. Both in the upper part of Fig. 3 and in Table II, it can be seen that neither the liquid phase nor any of the registered solids are stable with respect to the incommensurate structure. For the rest of nanotubes explored in this work, all the incommensurate solids considered will be of the type n-in-a-row, where n is the nanotube index.

In Fig. 3, we examine how the phase diagrams evolved when the tube radii increased. There, from top to bottom, we show the energy per particle of the different adsorbed phases on the (8,8), (10,10), and (12,12) tubes. As indicated above, for the (8,8) nanotube the ground state corresponds to an incommensurate solid. By increasing even more the tube radius we observe a progressive tendency towards stability of the liquid phase. In particular, our results reported in Table II indicate that the liquid phase absorbed on a (10,10) tube is essentially as stable as a ten-in-a-row solid, since their energies per particle are similar within their respective error bars. This is not true for the (12,12) cylinder, in which the ground state is clearly a liquid. A third-order polynomial fit to the liquid energies indicates that its equilibrium density is 0.0241 ± 0.0009 Å^{-2} and its energy per helium atom at this density -105.40 ± 0.02 K. A double-tangent Maxwell construction allows us to say that upon a density increase, a liquid at density $\rho = 0.0396 \pm 0.002$ Å^{-2} undergoes a first-order transition to a twelve-in-a-row solid whose lowest stable density is 0.0667 ± 0.003 Å^{-2}. The energies corresponding to the 2/5 and 3/7 commensurate structures, displayed as open diamonds and full triangles in Fig. 3, are bigger than those of the liquids with the same density, and therefore, unstable structures. We can also see that the curved equivalents to the $\sqrt{3} \times \sqrt{3}$ registered solid, whose energies per particle are displayed as full circles, are not stable either. The use of an anisotropic C-He potential in the (10,10) nanotube has basically the same effect than in the (5,5) one: it favors the stability of the incommensurate solid over the liquid, that now it is 0.57 ± 0.04 K less stable than a ten-in-a-row structure.

The other two cylinders considered, [(14,14) and (16,16)], have phase diagrams similar to that of the (12,12) tube. Their respective ground states are liquids with equilibrium densities and energies at equilibrium reported in Table III. The double-tangent Maxwell construction used in the (14,14) tube to obtain the limits of the transition zone between the liquid and the corresponding fourteen-in-a-row solid is shown in Fig. 4. The energy and density limits of the transition zones for those three tubes are given in Table III. All the commensurate solids (2/5,3/7, and $\sqrt{3} \times \sqrt{3}$) are unstable with respect both to the liquid and to the incommensurate solids in all the cylinders considered. This can be seen in Fig. 4 for the (14,14) nanotube, were their energies per particle are represented as an open

TABLE III. Energies per particle (e_g) and equilibrium ^{4}He densities (ρ_g) for tubes in which the ground state is a liquid. As before, the error bars are given in parenthesis and affect to the last figure shown. The upper stability limits for the liquids (ρ_u) and the lower densities for which the incommensurate solids are stable (ρ_l) are also given, together with their corresponding energies per particle.

Tube	ρ_g (Å^{-2})	e_g (K)	ρ_u (Å^{-2})	e_u (K)	ρ_l (Å^{-2})	e_l (K)
(12,12)	0.0241(9)	−105.40(2)	0.040(1)	−105.28(1)	0.067(1)	−105.05(2)
(14,14)	0.0189(9)	−106.01(2)	0.043(1)	−105.70(2)	0.060(1)	−105.42(5)
(16,16)	0.0260(1)	−105.85(2)	0.054(1)	−105.44(5)	0.066(1)	−105.15(4)

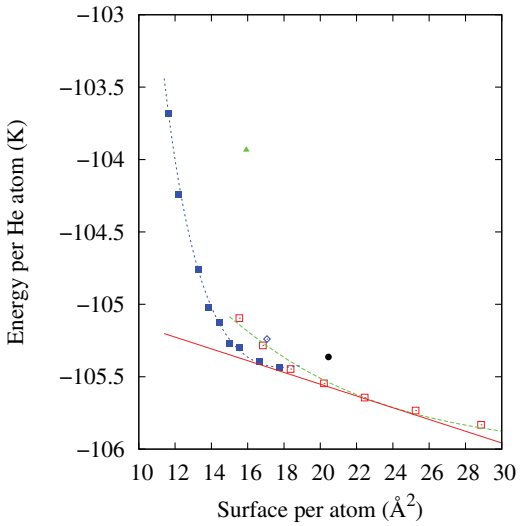

FIG. 4. (Color online) Double-tangent Maxwell construction solid line) used to obtain the limits of the transition zone between a liquid structure (dotted line, full squares), and an incommensurate one (dashed line, open squares). The meaning of the other symbols is the same as in Fig. 3.

diamond, a full triangle and a full circle, respectively. From Table III, we are also able to deduce that the equilibrium densities for the liquid phases (whose average density is $\sim$0.023 Å^{-2}) are much lower than their metastable counterpart in graphene[21] (0.044 Å^{-2}) and the same happens to the lowest stability limit of an incommensurate phase: an average of $\sim$0.064 Å^{-2} instead of the value 0.08 Å^{-2} of Ref. 21.

IV. CONCLUSIONS

Diffusion Monte Carlo calculations has allowed us to study the phase diagrams of ^{4}He adsorbed on carbon nanotubes of different radius. In principle, the ground state of this system should be a curved counterpart of the $\sqrt{3} \times \sqrt{3}$ structure found in graphite and graphene. This is what have been experimentally observed for heavier noble gases[10] adsorbed on wider tubes. In fact, any armchair nanotube (n,n) fulfills the necessary prescription for the formation of a seamless registered solid on it, i.e., its indexes (n,m) follow the restriction $(n-m)/3 = k$, k being an integer. However, as it can be inferred from the results of Table II, the ground state of ^{4}He on those tubes is either a liquid or an incommensurate solid, not a $\sqrt{3} \times \sqrt{3}$ arrangement. A comparison to the case of H_2 on the same substrates,[16] in which the $\sqrt{3} \times \sqrt{3}$ solid is the ground state for a (16,16) tube, indicates that, at least for the widest tubes considered, the weakness of the helium-helium and helium-carbon interactions are responsible for the lack of stability of that (or any other) commensurate structure.

Another relevant feature we have found is that for tubes whose radius is lower than $\sim$7 Å, the ground state is an incommensurate solid, whereas from the (12,12) tube up, the minimum energy structure corresponds to a liquid. This is probably a consequence of the above mentioned weakness in the helium interactions combined with the lower density of the curved $\sqrt{3} \times \sqrt{3}$ phase in comparison to planar graphene. Our results for the ^{4}He phase diagrams show a significant dependence on the curvature of the different tubes. As Table I shows, the energy in the infinite dilution limit for a (5,5) tube is $\sim$10 K larger than the same property for a (12,12) cylinder. This means that to obtain an energy per particle closer to the corresponding to a flat structure, one would have to increase more the number of helium neighbors of each adsorbed atom for a thinner tube than for a wider one. This leads to high densities and the formation of curved solids. These structures are incommensurate rather than registered because the necessary helium densities are higher than the corresponding to a $\sqrt{3} \times \sqrt{3}$ (or any other, see Table II) commensurate structure. For instance, in the (8,8) tube, the density of a $\sqrt{3} \times \sqrt{3}$ curved structure is 0.0412 Å^{-2} (see Table II), to be compared to 0.0636 Å^{-2} for the same arrangement on graphite and to 0.0744 Å^{-2} of the incommensurate solid on the same cylinder. However, when the diameter of the tube grows the curvature of the substrate is reduced and arrangements with lower densities, i.e., liquids, become stable.

ACKNOWLEDGMENTS

We acknowledge partial financial support from the Junta de de Andalucía Group PAI-205, Grant No. FQM-5985, MICINN (Spain) Grant Nos. FIS2010-18356 and FIS2011-25275, and Generalitat de Catalunya Grant 2009SGR-1003.

[1] A. C. Dillon, K. M. Jones, T. A. Bekkedahl, C. H. Kiang, D. S. Bethune, and M. J. Heben, Nature (London) **386**, 377 (1997).
[2] S. Talapatra, A. Z. Zambano, S. E. Weber, and A. D. Migone, Phys. Rev. Lett. **85**, 138 (2000).
[3] S. Talapatra, V. Krungleviciute, and A. D. Migone, Phys. Rev. Lett. **89**, 246106 (2002).
[4] W. Teizer, R. B. Hallock, E. Dujardin, and T. W. Ebbesen, Phys. Rev. Lett. **82**, 5305 (1999).
[5] T. Wilson, A. Tyburski, M. R. DePies, O. E. Vilches, D. Becquet, and M. Bienfait, J. Low Temp. Phys. **126**, 403 (2002).
[6] S. Ramachandran, T. A. Wilson, D. Vandervelde, D. K. Holmes, and O. E. Vilches, J. Low Temp. Phys. **134**, 115 (2004).
[7] J. V. Pearce, M. A. Adams, O. E. Vilches, M. R. Johnson, and H. R. Glyde, Phys. Rev. Lett. **95**, 185302 (2005).
[8] M. C. Gordillo, Phys. Rev. Lett. **101**, 046102 (2008).
[9] M. C. Gordillo, Phys. Rev. Lett. **96**, 216102 (2006).
[10] Z. Wang, J. Wei, P. Morse, J. G. Dash, O. E. Vilches, and D. H. Cobden, Science **327**, 552 (2010).
[11] M. M. Calbi, M. W. Cole, S. M. Gatica, M. J. Bojan, and G. Stan, Rev. Mod. Phys. **73**, 857 (2001).
[12] M. C. Gordillo, J. Boronat, and J. Casulleras, Phys. Rev. B **61**, R878 (2000).
[13] M. Rossi, D. E. Galli, and L. Reatto, Phys. Rev. B **72**, 064516 (2005).

[14]M. Rossi, D. E. Galli, and L. Reatto, J. Low Temp. Phys. **149**, 95 (2007).
[15]M. C. Gordillo, J. Boronat, and J. Casulleras, Phys. Rev. B **76**, 193402 (2007).
[16]M. C. Gordillo and J. Boronat, Phys. Rev. B **84**, 033406 (2011).
[17]S. Reich, C. Thompsen, and J. Maultzsch, *Carbon Nanotubes* (Wiley, Berlin, 2004).
[18]M. P. Gelfand and R. Lipowsky, Phys. Rev. B **36**, 8725 (1987).
[19]P. J. Upton, J. O. Indekeu, and J. M. Yeomans, Phys. Rev. B **40**, 666 (1989).
[20]E. S. Hernández, J. Low Temp. Phys. **137**, 89 (2004).
[21]M. C. Gordillo and J. Boronat, Phys. Rev. Lett. **102**, 085303 (2009).
[22]J. Boronat and J. Casulleras, Phys. Rev. B **49**, 8920 (1994).
[23]G. Stan and M. W. Cole, Surf. Sci. **395**, 280 (1998).
[24]R. A. Aziz, F. R. W. McCourt, and C. C. K. Wong, Mol. Phys. J. Chem. Phys. **61**, 1487 (1987).
[25]D. S. Greywall, Phys. Rev. B **47**, 309 (1993).
[26]M. C. Gordillo, J. Boronat, and J. Casulleras, J. Low Temp. Phys. **126**, 199 (2002).
[27]W. E. Carlos and M. W. Cole, Surf. Sci. **91**, 339 (1980).